Exchange Coupling in an Isostructural Series of Face-Sharing Bioctahedral Complexes $[LM^{II}(\mu\text{-}X)_3M^{II}L]BPh_4$ (M = Mn, Fe, Co, Ni, Zn; X = Cl, Br; L = 1,4,7-Trimethyl-1,4,7-triazacyclononane)

Ursula Bossek,[1a] Daniela Nühlen,[1a] Eckhard Bill,[1a] Thorsten Glaser,[1a] Carsten Krebs,[1a] Thomas Weyhermüller,[1a] Karl Wieghardt,*[,1a] Marek Lengen,[1b] and A. X. Trautwein[1b]

Max-Planck-Institut für Strahlenchemie, Stiftstrasse 34-36, D-45470 Mülheim an der Ruhr, Germany, and Institut für Physik, Medizinische Universität, D-23538 Lübeck, Germany

Received January 31, 1997[⊗]

The reaction of the divalent metal halides $ZnCl_2$, $ZnBr_2$, $MnCl_2{\cdot}4CH_3CN$, $MnBr_2$, $FeCl_2{\cdot}4CH_3CN$, $CoCl_2{\cdot}4CH_3CN$, $CoBr_2$, $NiCl_2{\cdot}6H_2O$, and $NiBr_2$, respectively, with the macrocycle 1,4,7-trimethyl-1,4,7-triazacyclononane (L) (1:1) in anhydrous acetonitrile, acetone, chloroform, or ethanol affords upon additon of $NaBPh_4$ the isomorphous series of complexes $[LM^{II}(\mu\text{-}X)_3M^{II}L]BPh_4$: **1**, M = Zn, X = Cl; **2**, Zn, Br; **3**, Mn, Cl; **4**, Mn, Br; **5**, Fe, Cl; **6**, Co, Cl; **7**, Co, Br; **8**, Ni, Cl; **9**, Ni, Br. Six of these complexes have been structurally characterized by single-crystal X-ray crystallography; they crystallize in the triclinic space group $P\bar{1}$ (No. 2) with $Z = 4$. Crystal data are as follows **1**, $a = 16.654(1)$, $b = 17.042(1)$, $c = 17.684(1)$ Å, $\alpha = 97.30(1)$, $\beta = 93.58(1)$, $\gamma = 117.46(1)°$; **3**, $a = 16.632(8)$, $b = 17.012(8)$, $c = 17.855(5)$ Å, $\alpha = 97.16(3)$, $\beta = 93.37(3)$, $\gamma = 117.24(3)°$; **5**, $a = 16.658(3)$, $b = 17.064(3)$, $c = 17.741(4)$ Å, $\alpha = 97.32(3)$, $\beta = 93.47(3)$, $\gamma = 117.36(3)°$; **6**, $a = 16.640(3)$, $b = 17.040(3)$, $c = 17.686(4)$ Å, $\alpha = 97.39(3)$, $\beta = 93.58(3)$, $\gamma = 117.39(3)°$; **8**, $a = 16.608(3)$, $b = 16.995(3)$, $c = 17.555(3)$ Å, $\alpha = 97.36(1)$, $\beta = 93.52(1)$, $\gamma = 117.52(1)°$; **9**, $a = 16.680(3)$, $b = 17.016(2)$, $c = 17.715(3)$Å, $\alpha = 96.99(1)$, $\beta = 93.70(1)$, $\gamma = 117.42(1)°$. All complexes consist of a dinuclear, face-sharing bioctahedral monocation with three μ_2-Cl or μ_2-Br bridging ligands and two LM fragments and well-separated tetraphenylborate anions (1:1). The cations cocrystallize in two different forms: an enantiomeric form with ($\lambda\lambda\lambda$) (or ($\delta\delta\delta$)) conformation at both LM fragments and a meso form with an ($\lambda\lambda\lambda$) conformation at one LM fragment and ($\delta\delta\delta$) at the other (ratio 1:1). From temperature-dependent magnetic susceptibility measurements (2−293 K) it was established that the spins of the unpaired electrons in **3** (d^5d^5 high spin), **4** (d^5d^5), **6** (d^7d^7 high spin), **7** (d^7d^7), **8** (d^8d^8), and **9** (d^8d^8) are intramolecularly, weakly *antiferromagnetically* coupled in each case. Surprisingly, the spins order *ferromagnetically* in **5** (d^6d^6 high spin). This is in contrast to the previously reported complex $[(thf)_3Fe^{II}(\mu\text{-}Cl)_3Fe^{II}(thf)_3][SnCl_5(thf)]$ (thf = tetrahydrofuran)[5] for which a new analysis of the temperature-dependence of the magnetic susceptibility and of field-dependent Mössbauer spectra establish a weak intramolecular *antiferromagnetic* coupling. The origin of this difference is analyzed.

Introduction

Dinuclear, face-sharing bioctahedral complexes of the type $[X_3M^{III}(\mu\text{-}X)_3M^{III}X_3]^{3-}$, where X represents the halides Cl^-, Br^-, and I^- and M^{III} is a trivalent first-, second- or third-row paramagnetic transition metal ion with d^n electronic configuration ($n = 1-3$), have played a key role in our understandig of molecular magnetic properties such as intramolecular exchange coupling phenomena and metal−metal bond formation.[2] Compounds of this type are well suited for such studies in the solid state because *intra*molecular spin exchange is in general significantly stronger than *inter*molecular interactions. In the first-row transition metal series these studies are focused on early transition metal ions Ti^{III}, V^{III},[3] and Cr^{III} with d^1, d^2, and d^3 configurations, respectively. It has been proposed that due to the close proximity of the two metal ions at 2.5−4.0 Å the dominant magnetic superexchange pathway within such a dinuclear cation is direct through-space which has also been described as incipient metal−metal bond formation.[4]

In contrast, reports on the magnetic properties of dinuclear complexes containing metal ions with d^n ($n \geq 4$) electronic configuration are rather scarce. Sobota et al. have in recent years synthesized three isostructural complexes of the type $[(thf)_3M^{II}(\mu\text{-}Cl)_3M^{II}(thf)_3]^+$, where thf is tetrahydrofuran and M^{II} represents Fe, Co, and Ni with high-spin d^6, d^7, and d^8 configurations,[5,6] respectively, and reported their structures and magnetic properties. Intramolecular, very weak antiferromagnetic coupling between the two paramagnetic metal ions has been established in each case by temperature-dependent magnetic susceptibility measurements; the results are summarized in Table 1.

We report here on an analogous but more comprehensive series of face-sharing bioctahedral complexes of the type $[LM^{II}(\mu\text{-}X)_3M^{II}L]BPh_4$, where L is the facially capping ligand 1,4,7-trimethyl-1,4,7-triazacyclononane, M^{II} represents the divalent metal ions Mn (high-spin d^5), Fe (high-spin d^6), Co (high-spin d^7), Ni (d^8), and Zn (d^{10}), and X is a single atom bridging ligand, chloride or bromide.

Chart 1 gives a list of these compounds and their labels. They crystallize in the triclinic space group $P\bar{1}$ with two crystallographically independent formula units ($Z = 4$). Due to the presence of three N-bound methyl groups at each macrocycle

⊗ Abstract published in *Advance ACS Abstracts*, June 1, 1997.

(1) (a) Max-Planck-Institut für Strahlenchemie. (b) Medizinische Universität Lübeck.
(2) Cotton, F. A.; Ucko, D. A. *Inorg. Chim. Acta* **1972**, *6*, 161 and references therein.
(3) Bouma, R. J.; Teuben, J. H.; Beukema, W. R.; Bansemer, R. L.; Huffman, J. C.; Caulton, K. G. *Inorg. Chem.* **1984**, *23*, 2715.
(4) Niemann, A.; Bossek, U.; Wieghardt, K.; Butzlaff, C.; Trautwein, A. X.; Nuber, B. *Angew. Chem., Int. Ed. Engl.* **1992**, *31*, 311.
(5) Janas, Z.; Sobota, P.; Lis, T. *J. Chem. Soc., Dalton Trans.* **1991**, 2429.
(6) Janas, Z.; Lis, T.; Sobota, P. *Polyhedron* **1992**, *11*, 3019.

S0020-1669(97)00119-5 CCC: $14.00

Table 1. Comparison of Structural and Magnetic Properties of Dinuclear Tris(μ-chloro)-Bridged Complexes

complex[a]	$M^1\cdots M^2$, Å	M−Cl_b, Å	Cl−M−Cl, deg	M^1−Cl−M^2, deg	J, cm^{-1} [b]	ref
$[V^{II}_2Cl_3(thf)_6]_2[Zn_2Cl_6]$	2.973(1)	2.477	87.3−88.0	73.8	−37.5	3, 4
$[Fe^{II}_2Cl_3(thf)_6][SnCl_5(thf)]$	3.086(2)	2.488(9)	85.0−86.2	76.7	−3	5
$[Co^{II}_2Cl_3(thf)_6][SnCl_5(thf)]$	n.d.	n.d.	n.d.	n.d.	−1.7	6
$[Ni^{II}_2Cl_3(thf)_6][SnCl_5(thf)]$	2.993(2)	2.403	84.9−86.4	77.0	−6.0	6
$[Ni^{II}_2Cl_3L'_2]BF_4\cdot CH_3CN$	2.921(2)	2.416	86.2−88.8	74.4	n.d.	12

[a] Abbreviations: n.d. = not determined; L′ = 1,4,7-trithiacyclononane; thf = tetrahydrofuran. [b] $H = -2J\vec{S}_1\vec{S}_2$.

Chart 1. Synthesized Complexes and Labels

$[L_2Zn_2(\mu\text{-}Cl)_3]BPh_4$	**1**	$[L_2Co_2(\mu\text{-}Cl)_3]BPh_4$	**6**
$[L_2Zn_2(\mu\text{-}Br)_3]BPh_4$	**2**	$[L_2Co_2(\mu\text{-}Br)_3]BPh_4$	**7**
$[L_2Mn_2(\mu\text{-}Cl)_3]BPh_4$	**3**	$[L_2Ni_2(\mu\text{-}Cl)_3]BPh_4$	**8**
$[L_2Mn_2(\mu\text{-}Br)_3]BPh_4$	**4**	$[L_2Ni_2(\mu\text{-}Br)_3]BPh_4$	**9**
$[L_2Fe_2(\mu\text{-}Cl)_3]BPh_4$	**5**		

L = 1,4,7-trimethyl-1,4,7-triazacyclononane; Ph = phenyl

and of the sterically very demanding diamagnetic tetraphenylborate anions, the individual cations are well separated in the solid state. They are magnetically dilute. Consequently, the electronic structure and the magnetic properties of these cations are readily studied in the solid state without interference of intermolecular electronic or magnetic interactions. Each metal ion is in a pseudo-octahedral environment comprising three facially coordinated tertiary amine nitrogens and the three bridging halide ions (Cl^- or Br^-). We were primarily interested in studying the intramolecular exchange coupling as a function of the metal−metal electronic configuration of the individual metal ion. More specifically, we intend with the present series of complexes to study the effect of a filled t_{2g}^6 set where a direct through-space interaction between the unpaired electrons is not possible, versus an incompletely filled t_{2g} subshell where such direct through-space interactions are possible.

An unexpected result of this investigation is the observation that in $[LFe^{II}(\mu\text{-}Cl)_3Fe^{II}L]BPh_4$ (**5**) an intramolecular *ferromagnetic* coupling prevails. This is in contrast to the complex $[(thf)_6Fe^{II}_2(\mu\text{-}Cl)_3][SnCl_5(thf)]$ reported by Sobota et al.[5] in which the two high-spin iron(II) ions are weakly antiferromagnetically coupled. Here we present a detailed magnetochemical and Mössbauer spectroscopic analysis of these two diferrous complexes.

Experimental Section

Preparation of Complexes. The following water-free starting complexes have been prepared according to published procedures:[7] $CoCl_2\cdot 4CH_3CN$, $FeCl_2\cdot 4CH_3CN$, $MnCl_2\cdot 4CH_3CN$, $MnBr_2\cdot 4CH_3CN$. The ligand 1,4,7-trimethyl-1,4,7-triazacyclononane (L) has been synthesized as described previously.[8] The preparation of complexes has been performed in water-free solvents and under an argon blanketing atmosphere. Sobota's complex has been synthesized according to the procedure given in ref 5.

$[L_2Zn_2(\mu\text{-}Cl)_3]BPh_4$ (1). A solution of $ZnCl_2$ (0.27 g, 2.0 mmol) in acetonitrile (60 mL) to which the ligand L (0.34 g, 2.0 mmol) was added was stirred at ambient temperature for 1.5 h. Addition of tetra-*n*-butylammonium tetraphenylborate (0.61 g, 1.0 mmol) initiated the slow precipitation (5 d) of colorless crystals which were collected by filtration. Yield: 0.72 g (40%). Anal. Calcd for $C_{42}H_{62}N_6Zn_2Cl_3B$ (898.95): C, 57.08; H, 8.09; N, 9.51. Found: C, 56.9; H, 7.5; N, 9.3.

$[L_2Zn_2(\mu\text{-}Br)_3]BPh_4$ (2). This complex was prepared as described for **1** by using $ZnBr_2$. Yield: 0.51 g (50%). Anal. Calcd for $C_{42}H_{62}N_6Zn_2Br_3B$ (1032): C, 48.88; H, 6.05; N, 8.81. Found: C, 49.3; H, 6.4; N, 8.5.

$[L_2Mn_2(\mu\text{-}Cl)_3]BPh_4$ (3). A solution of the ligand L (0.25 g, 1.46 mmol) and $MnCl_2\cdot 4CH_3CN$ (0.40 g, 1.41 mmol) in acetonitrile (30 mL) was stirred at 20 °C for 15 min. Addition of $NaBPh_4$ (0.5 g, 1.46 mmol) initiated the precipitation of colorless crystals. Yield: 0.35 g (34%). Anal. Calcd for $C_{42}H_{62}N_6Mn_2Cl_3B$ (878): C, 57.45; H, 7.11; N, 9.57; Cl 12.1. Found: C, 58.0; H, 7.3; N, 9.4; Cl, 11.5.

$[L_2Mn_2(\mu\text{-}Br)_3]BPh_4$ (4). This complex was prepared as described for **3** by using $MnBr_2$ as starting material.[9] Upon cooling the reaction mixture to 0 °C for 12 h colorless crystals were obtained. Yield: 0.30 g (60%). Anal. Calcd for $C_{42}H_{62}N_6Mn_2Br_3B$ (1011.4): C, 49.88; H, 6.18; N, 8.31. Found: C, 49.6; H, 6.3; N, 8.3.

$[L_2Fe_2(\mu\text{-}Cl)_3]BPh_4$ (5). This complex was prepared as described for **3** by using $FeCl_2\cdot 4CH_3CN$ as starting material. Pale yellowish crystals were obtained. Yield: 0.35 g (34%). Anal. Calcd for $C_{42}H_{62}N_6Fe_2Cl_3B$ (879.9): C, 57.33; H, 7.10; N, 9.55; Cl, 12.1. Found: C, 57.2; H, 7.2; N, 9.9; Cl, 12.2.

$[L_2Co_2(\mu\text{-}Cl)_3]BPh_4$ (6). To a solution of $CoCl_2\cdot 6CH_3CN$ (0.39 g; 1.0 mmol) and the ligand L (0.17 g; 1.0 mmol) in dry acetone (25 mL) was added $N_2H_4\cdot 2HCl$ (0.10 g). After the mixture was stirred for 2 h at 20 °C, a colorless precipitate was filtered off and $NaBPh_4$ (0.17 g) was added to the resulting blue solution: Within 3 d at 0 °C pink microcrystals precipitated. Yield: 0.19 g (43%). Anal. Calcd for $C_{42}H_{62}N_6Co_2Cl_3B$ (886.0): C, 56.94; H, 7.26; N, 9.49; Cl, 12.0. Found: C, 56.6; H, 7.1; N, 9.3; Cl, 11.8.

$[L_2Co_2(\mu\text{-}Br)_3]BPh_4$ (7). To a solution of $CoBr_2$ (0.22 g; 1.0 mmol) and the ligand L (0.17 g; 1.0 mmol) in chloroform (40 mL) was added a solution of $NaBPh_4$ (0.17 g) in acetone (15 mL). The stirred two-phasic solution was heated to reflux for 2.5 h after which time the reaction volume was reduced by evaporation to one-half. A violet microcrystalline solid formed. Yield: 0.46 g (90%). Anal. Calcd for $C_{42}H_{62}N_6Co_2Br_3B$ (1019.5): C, 49.49; H, 6.13; N, 8.24. Found: C, 50.3; H, 6.3; N, 8.3.

$[L_2Ni_2(\mu\text{-}Cl)_3]BPh_4$ (8). To a hot solution of $NiCl_2\cdot 6H_2O$ (0.43 g; 1.81 mmol) in an acetone/acetonitrile mixture (15 mL; 2:1 vol) were added 20 drops of ethyl orthoformate to remove the water. After addition of the ligand L (0.31 g; 1.81 mmol) the solution was refluxed until a clear green-blue solution was obtained. Addition of $NaBPh_4$ (0.31 g) initiated the precipitation of blue-green crystals. Yield: 0.60 g (75%). Anal. Calcd for $C_{42}H_{62}N_6Ni_2Cl_3B$ (885.6): C, 56.97; H, 7.06; N, 9.49; Cl, 12.0. Found: C, 56.8; H, 7.2; N, 9.4; Cl, 11.7.

$[L_2Ni_2(\mu\text{-}Br)_3]BPh_4$ (9). To a clear solution of $NiBr_2$ (0.22 g; 1.0 mmol) in dry ethanol (40 mL) was added the ligand L (0.17 g; 1.0 mmol) dissolved in ethanol (10 mL). The solution was refluxed for 1.5 h and $NaBPh_4$ (0.34 g) dissolved in ethanol (10 mL) was added. A green precipitate formed. Yield: 0.46 g (90%). Anal. Calcd for $C_{42}H_{62}N_6Ni_2Br_3B$ (1018.9): C, 49.50; H, 6.13; N, 8.24. Found: C, 49.1; H, 6.4; N, 8.0.

X-ray Crystallography. Crystal, data collection, and refinement parameters are given in Table 2. A colorless cubic crystal of **1** was placed on an Enraf-Nonius CAD4 diffractometer; a pale yellow crystal of **3**, a pale yellow crystal of **5**, a violet parallelepipede of **6**, and green parallelepipedes of **8** and **9** were placed on a Siemens P4 diffractometer. Graphite-monochromated Mo Kα radiation (λ = 0.710 73 Å) was used throughout. Intensity data were collected at 293 ± 2 K for **1**, **5**, **6**, **8**, and **9** and at 193 ± 2 K for **3**; they were corrected for Lorentz and polarization effects in the usual manner; correction for absorption effects was carried out for **1**, **5** and **9** by ψ-scans; for **6** and **8** no absorption correction was deemed necessary. The structures were solved by direct

(7) Hathaway, B. J.; Holah, D. G. *J. Chem. Soc.* **1964**, 2400.
(8) Wieghardt, K.; Chaudhuri, P.; Nuber, B.; Weiss, J. *Inorg. Chem.* **1982**, *21*, 3086.
(9) In this preparation extreme care must be taken that the solvent, the ligand L, and $MnBr_2$ are free of adventitious water. Otherwise varying amounts of $[LMn(\mu\text{-}Br)_2(\mu\text{-}OH)MnL]BPh_4$ cocrystallize.

Table 2. Crystallographic Data for Complexes $[L_2M_2(\mu\text{-}X)_3]BPh_4$[a]

	complex					
	1	**3**	**5**	**6**	**8**	**9**
empirical formula[b]	AZn_2Cl_3	AMn_2Cl_3	AFe_2Cl_3	ACo_2Cl_3	ANi_2Cl_3	ANi_2Br_3
fw	898.9	878.0	879.8	886.0	885.6	1018.9
a, Å	16.654(3)	16.632(8)	16.658(3)	16.640(3)	16.608(3)	16.680(3)
b, Å	17.042(3)	17.012(8)	17.064(3)	17.040(3)	16.995(3)	17.016(2)
c, Å	17.684(4)	17.855(5)	17.741(4)	17.686(4)	17.555(3)	17.715(3)
α, deg	97.30(3)	97.16(3)	97.32(3)	97.39(3)	97.36(1)	96.99(1)
β, deg	93.58(3)	93.37(3)	93.47(3)	93.58(3)	93.52(1)	93.70(1)
γ, deg	117.46(3)	117.24(3)	117.36(3)	117.39(3)	117.52(1)	117.42(1)
V, Å^3	4376(2)	4418(3)	4401.4(15)	4373.3(15)	4316.9(13)	4388.27(15)
μ, cm^{-1}	13.2	7.89	8.78	9.79	10.9	36.3
d(calcd), g cm^{-3}	1.33	1.32	1.33	1.35	1.36	1.54
T, °C	20	−80	20	20	20	20
R[c]	0.069	0.051	0.045	0.041	0.040	0.043

[a] Features common for all complexes: triclinic crystal system; space group $P\bar{1}$; $Z = 4$; radiation Mo Kα, $\lambda = 0.7101$ Å. [b] A = $C_{42}H_{62}N_6B$. [c] $R = \sum||F_o| - |F_c||/\sum|F_o|$.

and difference Fourier methods by using the SHELXTL-PLUS program package.[10] The function minimized during full-matrix least-squares refinement was $\sum w(|F_o| - |F_c|)^2$. The hydrogen atoms were placed at calculated positions with isotropic thermal parameters; the methyl groups were treated as rigid bodies. All non-hydrogen atoms were refined with anisotropic thermal parameters. It has not been possible to resolve the disorder of the methylene carbon atoms of the respective second monocation (involving metal ions M3 and M4) in all structures by a split atom model.

Physical Measurements. Electronic absorption spectra of complexes were measured in the range 350−2000 nm on a Perkin-Elmer Lambda 19 spectrophotometer in dry acetonitrile solution. The magnetic susceptibilities of powered samples of complexes were measured in the temperature range 2−293 K on a SQUID susceptometer (MPMS Quantum Design) at 1, 4, and 7 T. The Mössbauer spectra were recorded on alternating constant-acceleration spectrometer. The minimal experimental line width was 0.24 mm s^{-1} full-width at half-height. The sample temperature was maintained constant either in an Oxford Variox or an Oxford Mössbauer-Spectromag cryostat. The latter is a split-pair superconducting magnet system for applied fields up to 8 T where the temperature of the samples can be varied in the range 1.5−250 K. The field at the sample is oriented perpendicular to the γ-beam. The ^{57}Co/Rh source (1.8 GBq) was positioned at room temperature inside the gap of magnet system at a zero-field position. Isomer shifts are referenced relative to iron metal at 295 K.

Results

Syntheses. The crystalline salts $[L_2M_2(\mu\text{-}X)_3]BPh_4$ where L is the macrocycle 1,4,7-trimethyl-1,4,7-triazacyclononane, M is a divalent transition metal ion (Mn, Fe, Co, Ni, Zn), and X represents the bridging ligand chloride or bromide, were prepared from acetonitrile, acetone, chloroform or ethanol solutions of water-free halides MX_2 or their solvates $MX_2 \cdot 4CH_3CN$ by addition of 1 equiv of the macrocycle L and $Na[BPh_4]$, respectively. Upon evaporation of the solvents and standing of the solution under an argon blanketing atmosphere crystals of colorless zinc(II) (**1**, **2**), manganese(II) (**3**, **4**) and iron(II) (**5**), pink cobalt(II) (**6**, **7**), and blue-green nickel(II) compounds (**8**, **9**) were obtained in reasonable yields (50−70%). See Chart 1 for complexes and labels.

It is well established by single-crystal X-ray crystallography that in pseudo-octahedral mononuclear complexes LMX_3 the coordinated macrocycle L always adopts a conformation where the three five-membered chelate rings, $\overline{M-N-C-C-N}$, have either ($\lambda\lambda\lambda$) or ($\delta\delta\delta$) configuration, i.e. the LM fragment exists as racemate of two enantiomeric forms.[11] Consequently, the formation of the above dinuclear complexes leads, in principle, to two enantiomeric forms each of which contains two LM fragments of identical conformation, namely $[(\lambda\lambda\lambda)M^{II}(\mu\text{-}X)_3M^{II}(\lambda\lambda\lambda)]^+$ and $[(\delta\delta\delta)M^{II}(\mu\text{-}X)_3M^{II}(\delta\delta\delta)]^+$ and, in addition, the meso form $[(\delta\delta\delta)M^{II}(\mu\text{-}X)_3M^{II}(\lambda\lambda\lambda)]^+$, which is the achiral diastereomer. As we will show below by X-ray crystallography, the enantiomers and the meso form cocrystallize in the ratio 1:1.

Description of the Crystal Structures. The crystal structures of the isomorphous series of complexes **1**, **3**, **5**, **6**, **8,** and **9** have been determined by single-crystal X-ray crystallography. They crystallize in the triclinic space group $P\bar{1}$ with very similar unit cell parameters which are given in Table 2. There are four formula units $[L_2M_2(\mu\text{-}X)_3]BPh_4$, in the unit cell. Therefore, two such units are located on two different, crystallographically independent positions in each case. Table 3 summarizes selected bond distances, and Table 4 gives averaged bond angles.

Each structure consists of well-separated monocations $[L_2M_2(\mu\text{-}X)_3]^+$ and BPh_4^- anions. Both crystallographically independent monocations do not lie on any crystallographic symmetry element, and consequently, the dimensions of four independent octahedral LMX_3 units have been determined for each structure.

Before we discuss some pertinent structural features of individual monocations, we describe an interesting disorder phenomenon found in *all* structures under consideration here. We exemplify this by considering the structure **3** only, but the same observations apply for all structures. Figure 1 shows the structure of the two monocations $[L_2Mn_2(\mu\text{-}Cl)_3]^+$ with the individual atoms displayed as thermal ellipsoids drawn at the 40% probability level. A comparison of the two cations reveals that the ellipsoids of the methylene carbon atoms of the coordinated amines at Mn1 and Mn2 are significantly smaller than those of the coordinated macrocycle at Mn3 (and Mn4). More quantitatively, this observation is corroborated by the numerical values of the anisotropic (and isotropic U_{eq}) thermal parameters for these methylene carbon atoms (see Supporting Information). As a consequence, all C−C and C−N bond lengths of the 1,4,7-triazacyclononane backbone at Mn1 and Mn2 are normal single bonds and are observed in the usual range 1.51 ± 0.01 and 1.48 ± 0.01 Å, respectively. In contrast, due to apparently larger thermal motions of the methylene carbon atoms—at least at Mn3—the C−C bonds are unrealisti-

(10) Full-matrix least-squares structure refinement program package Siemens SHELXTL-PLUS: Sheldrick, G. M., (University of Göttingen, Göttingen, Germany.

(11) (a) Bhula, R.; Osvath, P.; Weatherburn, D. C. *Coord. Chem. Rev.* **1988**, *91*, 89. (b) Chaudhuri, P.; Wieghardt, K. *Prog. Inorg. Chem.* **1987**, *35*, 329.

Table 3. Selected Bond Distances (Å) of the Two Independent Cations in **1**, **3**, **5**, **6**, **8**, and **9**

	1	**3**	**5**	**6**	**8**	**9**
M1···M2	3.058(1)	3.077(2)	3.014(2)	3.048(2)	3.044(1)	3.234(1)
M1−X1	2.467(1)	2.536(2)	2.490(2)	2.464(2)	2.432(1)	2.591(1)
M1−X2	2.584(1)	2.557(2)	2.508(2)	2.489(2)	2.461(1)	2.622(1)
M1−X3	2.501(1)	2.503(2)	2.456(2)	2.443(2)	2.413(1)	2.566(1)
M2−X1	2.485(2)	2.526(2)	2.484(2)	2.463(2)	2.440(1)	2.595(1)
M2−X2	2.515(1)	2.587(2)	2.544(2)	2.525(2)	2.492(1)	2.655(1)
M2−X3	2.449(1)	2.556(2)	2.501(1)	2.477(1)	2.443(1)	2.589(1)
M1−N1	2.171(4)	2.284(4)	2.223(4)	2.180(4)	2.122(3)	2.133(6)
M1−N2	2.169(4)	2.274(5)	2.215(5)	2.161(5)	2.110(3)	2.101(7)
M1−N3	2.159(4)	2.281(4)	2.206(5)	2.170(5)	2.118(3)	2.132(6)
M2−N4	2.191(4)	2.254(4)	2.189(5)	2.142(4)	2.094(3)	2.106(6)
M2−N5	2.181(4)	2.269(4)	2.194(5)	2.153(5)	2.103(3)	2.107(6)
M2−N6	2.189(4)	2.266(3)	2.193(4)	2.149(3)	2.106(2)	2.107(4)
M3···M4	3.068(1)	3.078(2)	3.026(2)	3.062(2)	3.054(1)	3.243(1)
M3−X4	2.473(1)	2.531(2)	2.486(2)	2.461(2)	2.431(1)	2.588(1)
M3−X5	2.551(2)	2.522(2)	2.472(2)	2.460(2)	2.434(1)	2.574(1)
M3−X6	2.465(1)	2.570(2)	2.530(2)	2.508(2)	2.469(1)	2.629(1)
M3−N7	2.175(4)	2.263(4)	2.199(5)	2.154(4)	2.109(3)	2.103(5)
M3−N8	2.171(4)	2.270(4)	2.209(5)	2.157(5)	2.109(3)	2.121(6)
M3−N9	2.169(4)	2.258(5)	2.193(6)	2.160(5)	2.102(3)	2.103(7)
M4−X4	2.463(2)	2.526(2)	2.480(2)	2.458(1)	2.430(1)	2.585(1)
M4−X5	2.486(1)	2.558(2)	2.513(2)	2.492(2)	2.459(1)	2.601(2)
M4−X6	2.532(1)	2.536(2)	2.492(2)	2.470(2)	2.442(1)	2.603(1)
M4−N10	2.177(4)	2.268(4)	2.199(6)	2.159(5)	2.105(3)	2.110(6)
M4−N11	2.178(4)	2.262(5)	2.208(7)	2.165(6)	2.111(4)	2.119(8)
M4−N12	2.169(5)	2.273(3)	2.200(4)	2.157(4)	2.108(2)	2.096(5)

Table 4. Selected Averaged Bond Angles (deg) of One Independent[a] Cation in Crystals of **1**, **3**, **5**, **6**, **8**, and **9**

	1	**3**	**5**	**6**	**8**	**9**
N−M−N	82.7(2)	79.1(2)	81.2(1)	82.7(1)	84.3(1)	84.2(2)
N−M−X	95.4(1)	96.8(1)	95.7(1)	95.6(1)	95.2(1)	95.2(2)
X−M−X	86.5(1)	87.2(1)	87.3(1)	86.1(1)	85.4(1)	85.5(1)
M−X−M	75.4(1)	74.4(1)	74.2(1)	76.0(1)	76.9(1)	76.8(2)

[a] Values for the ordered enantiomeric form are given only.

cally short within the coordinated macrocycle (1.41 ± 0.01 Å). A conformational analysis of two sets of three five-membered chelate rings Mn−N−C−C−N at Mn1 and Mn2 reveals that both sets adopt the same conformation namely ($\lambda\lambda\lambda$)Mn1···Mn2($\lambda\lambda\lambda$) and its isomer ($\delta\delta\delta$)Mn1···Mn2($\delta\delta\delta$) which are related by a crystallographic inversion center in the space group $P\bar{1}$. This monocation is fully ordered. In contrast, the other monocation (Mn3, Mn4) appears to be disordered. It is not possible to determine the conformation of the three Mn3−N−C−C−N chelate rings. This can be understood if a superposition of a ($\lambda\lambda\lambda$)Mn and a ($\delta\delta\delta$)Mn fragment prevails at this site in the solid state as is schematically shown in Scheme 1 for one such ring. Note that the thermal parameters of the atoms of the $N_3Mn(\mu\text{-}Cl)_3MnN_3$ core in both cations are normal and it is meaningful to compare the metrical details of the two cores (see below). We propose that the monocation comprising the metal ions Mn3 and Mn4 actually consist of the achiral meso form $[(\lambda\lambda\lambda)Mn\cdots Mn(\delta\delta\delta)]^+$ which is superimposed by its "turned around" form $[(\delta\delta\delta)Mn\cdots Mn(\lambda\lambda\lambda)]^+$ in the solid state. *Thus crystals of* $[\{LM^{II}\}_2(\mu\text{-}X)_3][BPh_4]$ *cocrystallize as a mixture of their enantiomers and the meso form (1:1).*

In the following we briefly discuss the difference of the metrical details in the $N_3M(\mu\text{-}Cl)_3MN_3$ cores of the enantiomeric and the meso forms in the diferrous complex **5**. It is significant that the three Fe−Cl bond lengths within each $LFeCl_3$ octahedron are not equidistant; i.e. neither the ($\lambda\lambda\lambda$)Fe(μ-Cl)$_3$Fe($\lambda\lambda\lambda$) (or its enantiomer) nor the meso form ($\lambda\lambda\lambda$)Fe(μ-Cl)$_3$Fe($\delta\delta\delta$) possess C_3 (or higher) symmetry. The octahedra around Fe1 and Fe2 of the enantiomeric monocation are different: The sum of the three Fe1−Cl distances is 7.454 Å, and that of Fe2−Cl is larger at 7.529 Å (Δ = 0.075 Å). The same holds for the sums of Fe1−N and Fe2−N distances where the latter is now smaller (Σ, 6.644 Å, 6.576 Å; Δ = 0.068 Å). Note that the overall sum of Fe1−N and Fe1−Cl distances is 14.098 Å whereas that of Fe2−N and Fe2−Cl is 14.105 Å (Δ = 0.007 Å). In the meso form the two $LFeCl_3$ octahedra at Fe3 and Fe4 are more similar: The sum of the three Fe−Cl distances at Fe3 is 7.488 Å and at Fe4 7.485 Å and, similarly, the sum of the Fe−N distances (6.601 Å at Fe3 and 6.607 Å at Fe4; Δ = 0.006 Å). The $N_3Fe(\mu\text{-}Cl)_3FeN_3$ core of the meso form is more symmetric than that in the corresponding enantiomers. Interestingly, in the crystal structure of $[\{(thf)_3Fe^{II}\}_2(\mu\text{-}Cl)_3][SnCl_5(thf)]$[5] the $O_3Fe(\mu\text{-}Cl)_3FeO_3$ core also shows some degree of distortion but the Fe−Cl distances of both O_3FeCl_3 octahedra are within experimental error identical (average Fe−Cl: 2.488(9) Å). Note that the monocation in this structure also does not possess crystallographically imposed symmetry.

It should be pointed out that the observed different distortions of the enantiomeric and meso forms, of the $N_3M(\mu\text{-}X)_3MN_3$ cores are steric in nature rather than electronic. The relative orientations of the six methyl groups of the two macrocycles differ slightly in both forms, and more importantly, they are in close vicinity to the μ-chloro or μ-bromo bridges. This is nicely borne out by a comparison of the Ni−Cl bond distances in **8** and a similar complex $[L''_2Ni_2(\mu\text{-}Cl)_3][BF_4]\cdot CH_3CN$,[12] where L″ represents the macrocycle 1,4,7-trithiacyclononane. Thus

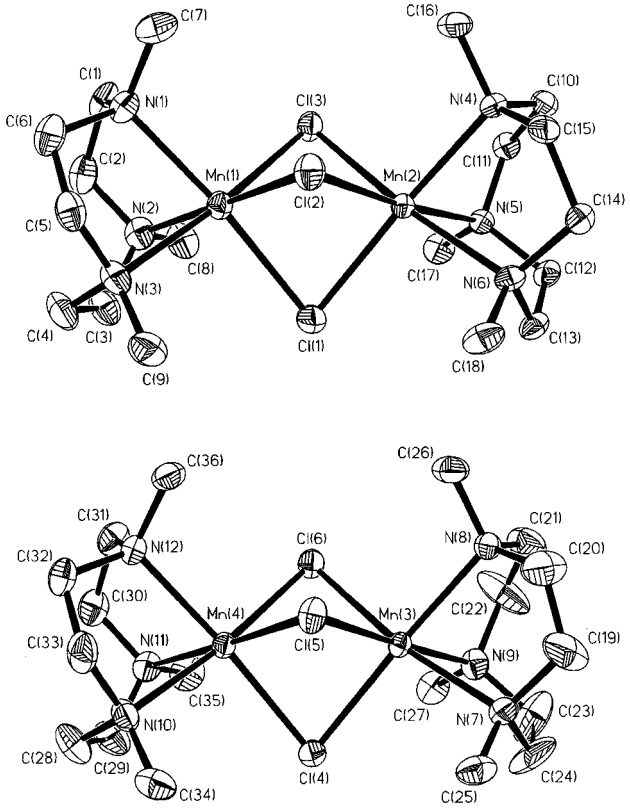

Figure 1. Structure of the two crystallographically independent monocations in crystals of **3**. The atoms are drawn at the 40% probability level.

Scheme 1

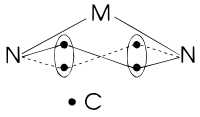

Table 5. Electronic Spectra of Complexes in Acetonitrile Solution (350−2000 nm) at 298 K

complex[a]	λ_{max}, nm (ϵ, L mol^{-1} cm^{-1})
6	1200 (6), 553 (sh), 523 (26)
7	1142 (33), 500 (80)
8	1053 (32), 633 (16), 387 (32)
9	1092 (34), 650 (30), 329 (70)

[a] Complexes **1**−**5** did not show absorption maxima with $\epsilon > 5$ L mol^{-1}cm^{-1} in the measured range.

the N−CH_3 groups in **8** are replaced by sterically less demanding thioether sulfur donors. The three Ni−Cl distances in **8** at Ni1 differ at 2.4313(1), 2.461(1), and 2.432(1) Å and similarly at Ni2 at 2.440(1), 2.492(1), and 2.443(1) Å. Even in the meso form with Ni−Cl distances at Ni3 of 2.431(1), 2.434(1), and 2.469(1) Å and at Ni4 of 2.430(1), 2.459(1), and 2.442(1) Å these differences prevail albeit to a lesser degree. In contrast, in $[L''_2Ni_2(\mu\text{-Cl})_3]^+$ four Ni−Cl distances are observed in the very narrow range of 2.419(3) to 2.411(3) Å and only one is slightly longer at 2.440(3) Å and one is shorter at 2.396(3) Å. Similarly, in $[(thf)_3Ni(\mu\text{-Cl})_3Ni(thf)_3][SnCl_5(thf)]$[6] the six Ni−Cl distances are within experimental error equidistant (average 2.403(6) Å).

Electronic Spectra and Magnetic Properties of Complexes. The electronic spectra of complexes have been recorded in the range 350−2000 nm in acetonitrile solution at ambient temperature; the results are given in Table 5. Compounds **1**−**5** are colorless and display no absorption in this range with $\epsilon > 5$ L mol^{-1} cm^{-1}. The pink complexes **6** and **7** exhibit typical weak d−d transitions of octahedral high-spin cobalt(II) (d^7) in the visible. Similarly, the spectra of **8** and **9** are typical of octahedral nickel(II) (d^8).

The temperature-dependence of the molar magnetic susceptibility of powdered solid samples of complexes **3**−**9** has been measured on a SQUID magnetometer in the range 2−298 K in an applied magnetic field of 1.0 T. The data were corrected for underlying diamagnetism by use of tabulated Pascal's constants; no correction for temperature-independent paramagnetism was applied.

The data were fitted to the isotropic Heisenberg, Dirac, van Vleck (HDvV) model by using the spin Hamiltonian in eq 1,

$$H = -2J\vec{S}_1\cdot\vec{S}_2 + \sum_{i=1}^{2}\left\{D_i\left[S_{iz}^{\,2} - \frac{S_i(S_i+1)}{3}\right] + \mu_B g_i \vec{S}_i\cdot\vec{B}\right\} \quad (1)$$

which consists of a HDvV exchange, a zero-field splitting, and Zeeman term. All symbols in eq 1 have their usual meaning. Since the dinulear complexes have approximately C_3 symmetry, the rhombicity, E/D, is considered to be zero. The parameters were optimized to fit optionally either χ_M or $\chi_M T$ as a function of temperature because the fits of χ_M are very sensitive to traces of paramagnetic (mononuclear) impurities (PI). Their contributions are included in the best fits shown in Figures 2−4; numerical results are summarized in Table 6. Figure 2 shows the temperature-dependence of the magnetic moment, μ_{eff}, per dinuclear unit for complexes **3**−**5**. Moderately strong intramolecular antiferromagnetic coupling is observed in the manganese(II) complexes **3** and **4**. The g value obtained from the above fitting procedure for **4** is not reliable. This unrealistic value is probably due to the presence of a dinuclear impurity such as $[LMn(\mu\text{-OH})(\mu\text{-Br})_2MnL]BPh_4$ which we have isolated from acetonitrile/water mixtures and which we will report separately.[9]

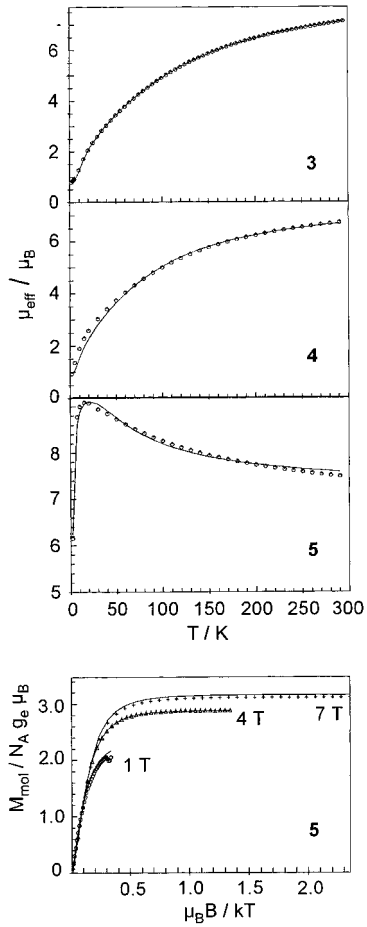

Figure 2. Temperature dependence of the magnetic moment, μ_{eff}, per dinuclear unit of powdered samples of complexes **3**−**5** measured at 1 T. Bottom: Magnetization data of **5** measured at various fields. The solid lines represent best fits to the spin-Hamiltonian eq 1 with parameters listed in Table 6.

Complex **5** exhibits weak *ferromagnetic* coupling between the two high-spin ferrous ions of the monocation. Figure 2 (bottom) shows the magnetization M in $Ng_e\mu_B$ units as a function of $\mu_B B/kT$ measured at three different applied magnetic field strengths (1, 4, and 7 T). The solid lines represent best fits obtained by using the parameter set in Table 6 for **5**. The $S_t = 4$ ground state of **5** is confirmed by this fit. As a consequence of the zero-field splitting the magnetization data cannot be fit to a simple Brillouin function. From the fit shown in Figure 2 (bottom) the sign and the magnitude of the zero-field parameter D was established to be $+5.5$ cm^{-1}. A calculated error contour map of J vs D showed two minima with identical J values. The global minimum was found at $D = +5.5$ cm^{-1} whereas a local minimum had $D = -2.4$ cm^{-1} but with a much larger error. It is not possible to fit the magnetization data satisfactorily with $D = -2.4$ cm^{-1}.

Compounds **6** and **7** contain octahedral high-spin cobalt(II) ions with a T ground state (in O_h symmetry), which is split in C_{3v} local symmetry into A and E. This splitting affects a quenching of the first-order orbital momentum. If this splitting is large the orbital momentum contributes by several tens of wavenumbers to D and induces a strong anisotropy of the **g** tensor.[13] It is therefore justified to use eq 1 to fit the susceptibility data of **6** and **7**. This is shown in Figure 3. For both compounds very satisfactory fits were obtained. It is noted that the value of J is not very sensitive to variation of $|D|$

(12) Blake, A. J.; Halcrow, M. A.; Schröder, M. *Acta Crystallogr.* **1992**, *C48*, 1844.

(13) Kahn, O. *Molecular Magnetism*; VCH Publishers: New York, 1993; p 208.

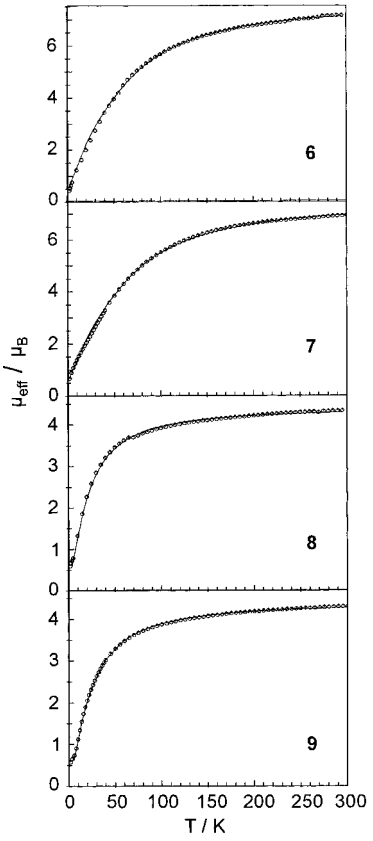

Figure 3. Temperature dependence of the magnetic moment, μ_{eff}, per dinuclear unit of powdered samples of complexes **6**−**9**. The solid lines represent best fits obtained as described in Figure 2.

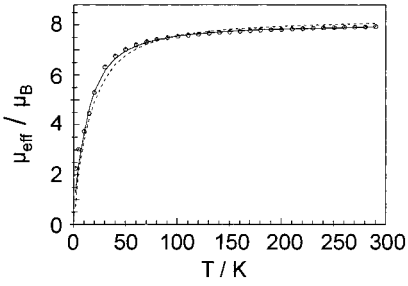

Figure 4. Temperature dependence of the magnetic moment, μ_{eff}, per dinuclear unit of a powdered sample of $[(thf)_6Fe^{II}_2(\mu\text{-}Cl)_3][SnCl_5(thf)]$. The solid line represents the best fit to eq 1 with parameters listed in Table 6. The dashed line was calculated by using the spin-Hamiltonian $H = -2J\vec{S}_1\vec{S}_2$ ($S_1 = S_2 = 2$) and Sobota's published parameters $J = -3$ cm^{-1} and $g = 2.4$.

Table 6. Magnetic Properties of Complexes

complex	J, cm^{-1} [a]	g[b]	PI, %[c]	D, cm^{-1} [d]
3	−11.6	2.07	1.8 ($S = 5/2$)	0 (fixed)
4	−8.5	1.84	2.7 ($S = 5/2$)	0 (fixed)
5	+5.8	2.08	0	+5.5
6	−13.1	2.86	0	±40 (fixed)
7	−13.3	2.80	1.4 ($S = 3/2$)	±40 (fixed)
8	−10.5	2.26	4.5 ($S = 1$)	±10 (fixed)
9	−12.0	2.25	4.1 ($S = 1$)	±10 (fixed)

[a] Coupling constant ($H = -2J\vec{S}_1\vec{S}_2$). [b] g value (fit parameter). [c] Percentage of a monomeric paramagnetic impurity with its assumed spin in parentheses. [d] Zero-field-splitting parameter.

between 35 and 45 cm^{-1}; it changes by ± 0.2 cm^{-1} in this range of $|D|$. Therefore, we have fixed D at 40 cm^{-1} in the fitting procedure; the sign of D cannot be determined from these data. Both compounds **6** and **7** are intramolecularly antiferromagnetically coupled.

Octahedral nickel(II) in **8** and **9** exhibits, in general, non-negligible zero-field splitting. As described above the fit of the temperature-dependent susceptibility data is not very sensitive to variations of $|D|$ in the range 5−25 cm^{-1}. Therefore, we have fixed the value for D at 10 cm^{-1}. The resulting fits are excellent. Both complexes show intramolecular antiferromagnetic coupling.

In order to compare the magnetic properties of **5** with those reported by Sobota et al.[5] for $[(thf)_6Fe^{II}_2(\mu\text{-}Cl)_3][SnCl_5(thf)]$, we have prepared a fresh sample of this compound and measured its temperature-dependent susceptibility. The data are shown in Figure 4. Clearly, the effective magnetic moment decreases with decreasing temperature indicating a *diamagnetic* ground state ($S_t = 0$). A fit of the data using the simple spin-Hamiltonian $H = -2J\vec{S}_1\vec{S}_1$ ($S_1 = S_2 = 2$) with g and J being the only variables is possible and has been reported by Sobota et al.[5] (They do not show their data.) These authors arrive at $J = -3$ cm^{-1} and $g = 2.4$. The fit obtained by using these parameters to our data is shown as dotted line in Figure 4—a reasonable but not excellent fit. By using the spin-Hamiltonian eq 1 including zero-field splitting the fit was improved considerably. We obtain g and J values of 2.34 and −2.3 cm^{-1}, respectively, with $|D|$ values in the range 1−4 cm^{-1}.

By using these parameters with a *positive D* only the correct trend in the field-dependent magnetization data measured at 1, 4, and 7 T (not shown) can be reproduced. At low temperatures (2−10 K) the fits do not agree well. Inclusion of a paramagnetic impurity of ∼11% $[LFe^{III}Cl_3]$ did improve the fit, but this is not corroborated by the zero-field Mössbauer spectra (see below) which rule out such large amount of Fe^{III} in the sample.

The relatively large g value of 2.34 points to significant zero-field splitting. From error contour maps of J over D steep local minima of the error were obtained for small (+2 cm^{-1}) and large (−60 cm^{-1}) values of D. Excluding the minima at large zero-field splitting—in agreement with the field-dependent Mössbauer spectra—it appears that in Sobota's complex zero-field splitting and spin coupling are of the same order of magnitude ($D = +1$ to +4 cm^{-1}; $J = -1$ to −3 cm^{-1}). Using these parameters and a g value at 2.3, an excellent fit of the temperature-dependent susceptibility data is obtained, but as pointed out, the magnitization data are not reproduced in every detail.

In summary, the above analysis allows two important conclusions to be drawn: In Sobota's complex the two ferrous ions are weakly antiferromagnetically coupled and the local zero-field splitting parameter D is positive and of the same order of magnitude as the coupling constant J.

Mössbauer Spectroscopy. Zero-field Mössbauer spectra of **5** and Sobota's complex are displayed in Figure 5; the corresponding Mössbauer parameters are given in Table 7.

The zero-field spectrum of crystalline **5** at 4.2 K consists of a broad quadrupole doublet with distinct shoulders which suggest the presence of essentially three different subspectra (Figure 5A,B). Numerical fits with three Lorentzian doublets yielded intensity ratios of 1:2:1. The "nested" arrangement of these subspectra with similar isomer shifts but different quadrupole splittings is in agreement with the differing bonding situation at each $LFeCl_3$ octahedron of the two monocations in the solid state of **5**; they are typical of octahedral Fe^{II} ($3d^6$ high spin). At a given temperature the quadrupole splittings, ΔE_Q, scatter in the range 0.98−2.08 mm s^{-1}. In addition, for two of the subspectra ΔE_Q is significantly temperature dependent which indicates either thermal population of close lying excited spin−orbital states or temperature-dependent structure variations. The zero-field Mössbauer spectrum of Sobota's complex is remark-

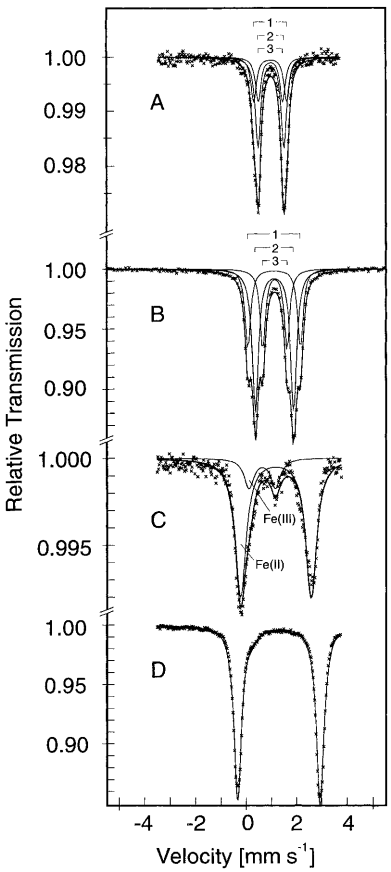

Figure 5. Zero-field Mössbauer spectra of **5** (A, B, powder sample at 295 K and 4.2 K, respectively; C, acetonitrile solution at 80 K) and $[(thf)_6Fe^{II}_2(\mu\text{-}Cl)_3][SnCl_5(thf)]$ (D, powder sample at 4.2 K). The experimental data in (C) are corrected for precipitated microcrystals of **5** (21%); the subspectra of the solid were subtracted by using the 77 K parameters given in Table 7.

Table 7. Mössbauer Parameters of **5** (Crystalline and in CH_3CN Solution) and of Crystalline $[(thf)_6Fe^{II}_2(\mu\text{-}Cl)_3][SnCl_5(thf)]$

		temp, K				
	param[a]	4.2	77	160	295	rel intensity
subspectrum 1[c] of **5**	δ	1.10	1.08	1.05	0.96	25%
	ΔE_Q	2.08	1.86	1.57	1.31	
subspectrum 2[c] of **5**	δ	1.10	1.09	1.06	0.98	50%
	ΔE_Q	1.52	1.33	1.23	1.03	
subspectrum 3[c] of **5**	δ	1.13	1.10	1.07	0.97	25%
	ΔE_Q	0.96	0.92	1.03	0.97	
CH_3CN soln of **5**	δ	1.16[b]				~100%
	ΔE_Q	2.79[b]				
$[(thf)_6Fe_2Cl_3]$ $[SnCl_5(thf)]$	δ	1.30	1.29[b]			
	ΔE_Q	3.26	3.22[b]			

[a] Isomer shift, δ (referenced vs α-Fe at 295 K), and quadrupole splitting, ΔE_Q, in mm s^{-1}, respectively. [b] Measured at 80 K. [c] See Figure 5.

ably different (Figure 5D). It shows only one doublet with δ = 1.3 mm s^{-1} and a large quadrupole splitting ΔE_Q = 3.27 mm s^{-1} at 4.2 K although it is noted that the spectrum shows a slight asymmetry and a relatively large line width of Γ = 0.36 mm s^{-1} which indicates some degree of microheterogeneity. The enormous differences in ΔE_Q suggest the presence of different electronic ground states in **5** and Sobota's complex.

Interestingly, the Mössbauer spectrum of **5** measured in CH_3CN *solution* also displays a large quadrupole splitting of 2.8 mm s^{-1} at 80 K as shown in Figure 5C. Furthermore, the Fe^{II} sites of the meso form and of the enantiomers become indistinguishable as only one subspectrum is detected.

Table 8. Expectation Values of the Valence Contributions to the Electric Field Gradient Tensor $(EFG)_{val}$ for 3d Orbitals in C_{3v} Symmetry with a_1 Ground State[a]

		V_{xx} $e\langle r^{-3}\rangle$	V_{yy} $e\langle r^{-3}\rangle$	V_{zz} $e\langle r^{-3}\rangle$
2e	$\left\{\begin{matrix}\sqrt{1/3}\,\lvert x^2-y^2\rangle+\sqrt{2/3}\,\lvert yz\rangle\\ \sqrt{1/3}\,\lvert xy\rangle-\sqrt{2/3}\,\lvert xz\rangle\end{matrix}\right\}$			
1e	$\left\{\begin{matrix}\sqrt{2/3}\,\lvert x^2-y^2\rangle-\sqrt{1/3}\,\lvert yz\rangle\\ \sqrt{2/3}\,\lvert xy\rangle+\sqrt{1/3}\,\lvert xz\rangle\end{matrix}\right\}$	0 -2/7	-2/7 0	+2/7 +2/7
a_1	$\lvert z^2\rangle$	+2/7	+2/7	-4/7

[a] The orbital functions are expressed as linear combinations of the usual $|ij\rangle$ d functions in octahedral symmetry.[23] The tensor elements for the basic orbitals $|ij\rangle$ are taken from ref 24. In order to convert the elements of $(EFG)_{val}$ to quadrupole splitting multiply by 4.2 mm s^{-1}/$(4/7)e\langle r^{-3}\rangle$. Note that the molecular *z*-axis is taken collinearly to the 3-fold axis in C_{3v}.

For solid **5** and Sobota's complex the sign of the main component, V_{zz}, of the electric field gradient tensor (EFG) and asymmetry parameter, η,[14] were unambiguously determined from high-field Mössbauer measurements at elevated temperatures (120 and 180 K; 3.5 and 7 T applied field). These spectra are not shown. For both compounds V_{zz} is negative and η is zero with an experimental error of less than 0.1. The same results should apply for **5** in solution. With the reasonable assumption that the EFG of the Fe^{II} sites is dominated by the nonspherical valence charge distributions[14] this result indicates a d_{z^2}-type ground-state orbital for the sixth d electron which exceeds the "spherical" half-filled d-shell. From corresponding $(EFG)_{val}$ tensor elements listed in Table 8 it is then obvious that out of the possible ground state functions a_1 and 1*e* in (approximate) C_{3v} symmetry only a_1 yields a large negative expectation value for V_{zz} (as is observed). Taking $V_{zz} = -4/7e\langle r^{-3}\rangle$, $\langle r^{-3}\rangle = 5a_0^{-3}$, and $Q = 0.15b$ for a hypothetical pure valence contribution from a_1 and neglecting covalency and lattice contributions to the EFG, one would arrive at a quadrupole splitting of $\Delta E_Q = -4.2$ mm s^{-1}.[15] Since the ΔE_Q values of **5** in solution and even more of Sobota's complex in the solid state approach this theoretical value, we *postulate for both complexes a relatively isolated a_1 ground state for the Fe^{II} sites.* On the other hand, the reduced quadrupole splittings of solid **5** then owe their origin to distortions of local C_3 symmetry which perturb the splitting of the d orbitals and induce spin−orbit mixing of a_1 and 1*e* states and thereby add positive contributions to V_{zz}. An estimate based on the $(EFG)_{val}$ components given in Table 8 shows that mixing of only 15% 1*e* contributions into the a_1 ground state is sufficient to reduce ΔE_Q to −1.5 mm s^{-1} (with η = 0.06). This is close to the experimental results for solid **5**. *Thus it is quite plausible that the distortions observed in the molecular structure of solid **5** induce perturbations of the electronic structure.*

It is now possible to assign the different Mössbauer subspectra of solid **5** to individual Fe^{II} sites (Fe1···Fe4) in the crystal of **5** by crude quantitation of the local deviations (i) from ideal C_3 (C_{3v}) symmetry and (ii) from the the Fe−Cl bond length of 2.488 Å in $[Fe_2(thf)_6Cl_3][SnCl_5(thf)]$. To this end we have calculated (i) a distortion parameter Δ_1 for each Fe^{II} site by summing up the squares of deviations of the individual Fe−Cl

(14) Gütlich, P. In *Mössbauer Spectroscopy*, Gonser, U., Ed.; Springer-Verlag: Berlin, Heidelberg, New York, 1975; p 53.
(15) (a) Lauer, S.; Marathe, V. R.; Trautwein, A. X. *Phys. Rev.* **1979**, *A19*, 1852. (b) Bominaar, E. L.; Guillin, J.; Sawaryn, A.; Trautwein, A. X. *Phys. Rev.* **1989**, *B39*, 72.

Table 9. Assignment of the Mössbauer Subspectra to Fe(II) Sites in Crystalline **5** at 295 K

Fe^{II} site[a]	Δ_1, 10^{-3} Å^{2} [b,c]	Δ_2, 10^{-2} Å[d]	subspectrum[e]	ΔE_Q, mm s^{-1} [f] (at 4.2 K /295 K)
Fe1	1.39	−0.4	2 (25%)	1.52/1.03
Fe2	1.91	+2.1	3 (25%)	0.96/0.97
Fe3	1.83	+0.8	2 (25%)	1.52/2.03
Fe4	0.56	+0.7	1 (25%)	2.08/1.31

[a] Labels as in Table 3 and Figure 1 (replace Mn for Fe). [b] $\Delta_1 = \sum_{i=1}^{3}(d_{Fe-Cl(i)} - \langle d_{Fe-Cl}\rangle)^2$; $\langle d_{Fe-Cl}\rangle = {}^1/_3\sum_{i=1}^{3} d_{Fe-Cl(i)}$. The bond lengths $d_{Fe-Cl(i)}$ are taken from Table 3. [c] Note that the calculated Δ_1 values for the two iron sites in $[(thf)_6Fe_2(\mu\text{-}Cl)_3][SnCl_5(thf)]$ are smaller: 0.05×10^{-3} and 0.33×10^{-3} Å^{-2}. [d] $\Delta_2 = \langle d_{Fe-Cl}\rangle - 2.488$ Å, with 2.488 Å being the average Fe−Cl distance in $[Fe_2(thf)_6Cl_3][SnCl_5(thf)]$. [e] See Figure 5. [f] Quadrupole splittings from Table 7.

bond length, $d_{Fe-Cl(i)}$, from the average Fe−Cl bond length, $\langle d_{Fe-Cl}\rangle$, and a corresponding parameter Δ_2 for each Fe^{II} site by taking the difference between $\langle d_{Fe-Cl}\rangle$ and 2.488 Å. The results are shown in Table 9. The smaller the deviation parameters Δ_1 and Δ_2 the larger $|\Delta E_Q|$ should be according to the arguments presented above. At 4.2 and 295 K one of the Mössbauer subspectra in Figure 5A which accounts for one iron site (subspectrum 1 with 25% relative intensity) has a significantly larger ΔE_Q than the other two subspectra which accout for three other sites (50% + 25% relative intensity). The deviation parameters Δ_1 and Δ_2 are significantly larger for Fe4 than those of Fe1, Fe2, and Fe3. Therefore, we assign subspectrum 1 (Figure 5A) to Fe4 of the meso form of one of the monocations in **5.** For Fe2 this reasoning is opposite: Large deviation parameters result in stronger spin−orbit mixing and, therefore, in strongly reduced ΔE_Q. Hence, we assign subspectrum 3 to Fe2. The remaining subspectrum 2 then represents the practically unresolved overlaps of signals from sites Fe1 and Fe3.

The magnetic Mössbauer spectra of Sobota's complex provided further insight into the zero-field and exchange interactions of this compound which proved to be helpful resolving the ambiguities of the analysis of the magnetic susceptibility data (see above). We have measured these spectra in a wide temperature range (1.7−120 K). In weak or moderately strong fields (1−4 T) the spectra showed only weak magnetic splittings due to partial cancellation of internal and applied fields. Resolved magnetic hyperfine lines were only observed in a strong field of 7 T. This observation is fully consistent with a weak intramolecular antiferromagnetic interaction of the iron(II) spins and a positive zero-field splitting yielding locally almost nonmagnetic "$m_{s,i} = 0$" ground levels. Spin-Hamiltonian simulations for the strong field case revealed a pronounced sensitivity on the parameters D and J which is indicative of delicate mixing of magnetic substates by coupling zero-field and exchange interactions. The "best results" of these spin-Hamitonian simulations, obtained for the series of measured Mössbauer spectra by adopting identical iron sites with the constraint $E/D = 0$, are shown in Figure 6. Despite the fact that some details of the fits are poor, the essential features of the spectra, i.e. the magnetic splittings for a wide temperature range, are satisfactorily reproduced. This lends confidence to the derived mixed nature of the spin ground level and the sequence of substates; the D and J values obtained should, therefore, be essentially correct.

The misfits of the spectral pattern are related to the high sensitivity of the hyperfine splittings toward marginal variations of D, E/D, and J. Such variations are easily induced by strain on the Fe^{II} sites in the powder crystallites. For instance, missing absorptions in the simulations could be corrected by allowing for inhomogeneous spectral contributions with $0 < E/D < 0.1$.

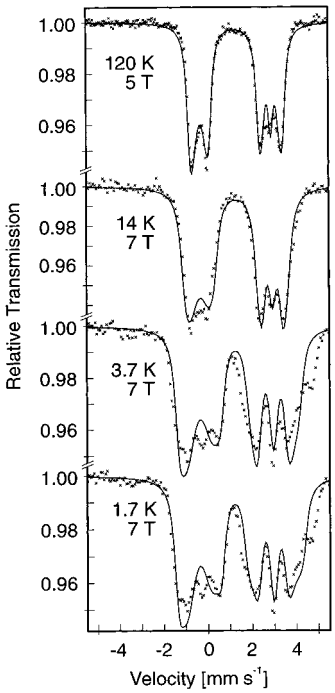

Figure 6. Magnetic Mössbauer spectra of solid $[(thf)_6Fe^{II}_2(\mu\text{-}Cl)_3][SnCl_5(thf)]$. The solid lines represent spin-Hamiltonian simulations with $S_i = 2$, $\eta = 0$; $J = -0.8$ cm^{-1}, $D_i = +3.5$ cm^{-1}, $g = 2.0$; $\bar{A}_i/g_N\mu_N = (-1.0, -10.2, -19.7)$T, ; $\Delta E_Q = -3.27$ mm s^{-1} (-3.19 mm s^{-1} at 120 K), and $\delta = 1.3$ mm s^{-1} (1.27 mm s^{-1} at 120 K).

Due to the increasing ambiguities we refrained from extending the parameter set.

The spin-Hamiltonian parameters obtained in this fashion from magnetic Mössbauer spectroscopy do not perfectly match the set obtained from the analysis of the magnetic susceptibility. We attribute this to the differing sensitivity of both methods toward sample inhomogeneities. However, the Mössbauer simulations do allow us to limit the parameter set to the range $0 < D < +5$ cm^{-1} and $-0.5 > J > -2$ cm^{-1}.

Discussion. For bioctahedral face-sharing complexes containing two $3d^3$ paramagnetic ions the observed exchange coupling is invariably antiferromagnetic. An empiral correlation between the M···M distance and the magnitude of the coupling constant J shows that the latter is not greatly affected by the nature of the three bridging ligands (O^{2-}, HO^-, EtO^-, Cl^-, Br^-, J^-) or the metal ion (V^{II}, Cr^{III}, Mn^{IV}).[4] It was concluded that in face-sharing complexes with d^3-d^3 configurations no magnetic superexchange mediated by bridging ligands occurs but rather a direct metal−metal interaction (overlap of a_1 orbitals) dominates. This is in excellent agreement with extended Hückel MO calculations by Leuenberger and Güdel[16] for $[Cr^{III}_2X_9]^{3-}$ complexes (X = Cl, Br, I) and, more recently, ab initio calculations by Ceulemans et al.[17] on $[Ti^{III}_2Cl_9]^{3-}$ (a d^1−d^1 system). These theoretical papers show that the dominant contribution to the exchange interaction in these systems arises from the direct interaction of the a_1 orbitals (t_{2g} in octahedral symmetry).

Keeping these results in mind, we now attempt to rationalize the exchange pathways in bioctahedral face-sharing complexes containing two first-row transition metal ions with metal−metal ($n = 5$−8) configuration. For the manganese(II) complexes (d^5 high spin) **3** and **4** additional superexchange paths via the

(16) Leuenberger, B.; Güdel, H. U. *Inorg. Chem.* **1986**, *25*, 181.
(17) Ceulemans, A.; Heylen, G. A.; Chibotaru, L. F.; Maes, T. L.; Pierloot, K.; Ribbing, C.; Vanquickenborne, L. G. *Inorg Chim. Acta* **1996**, *251*, 15.

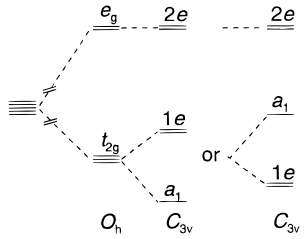

Figure 7. Splitting caused by a trigonal distortion (C_{3v}) superposed on an octahedral field.[23]

half-occupied e_g orbitals must be considered. In contrast, for the nickel(II) complexes **8** and **9** a direct metal−metal interaction is not possible because the metal ion t_{2g} orbitals are filled. In the cobalt(II) complexes **6** and **7** both possibilities are available. Notwithstanding the fine details in all of these complexes the exchange coupling is always antiferromagnetic. Thus the ferromagnetically coupled iron(II) complex **5** in conjunction with Sobota's antiferromagnetically coupled complex represent test cases for any consistent interpretation of the exchange coupling in complexes containing this structural motif.

The tris(μ-chloro)-bridged complex **3** as well as its tris(μ-bromo)-bridged analog **4** display a weak antiferromagnetic coupling of similar magnitude. The slightly diminished coupling in **4** as compared to **3** might be explained by the expected increase of the metal···metal distance on substituting the chloro for bromo bridges (see the structural changes in **8** and **9**) and the resulting diminished overlap integral of the a_1 orbitals.

Interestingly, the antiferromagnetic exchange coupling in **9** is stronger than in **8** despite the fact that the Ni··Ni distance in **9** at 3.234 Å is longer than in **8** at 3.044 Å. As pointed out above the direct metal−metal interaction via a_1 orbitals can be ruled out because the only available magnetic orbitals of the octahedral Ni^{II} ions are e_g orbitals. In **8** and **9** a σ-superexchange via bridging halide ions prevails and overlap of the e orbitals with a filled p orbital of the bridge is slightly stronger (more covalent) for the bromo complex **9** than for the chloro species **8**.[18] The Ni−Br−Ni and Ni−Cl−Ni angles at 76.9 and 76.8°, respectively, are similar and much smaller than 90°. It is noted that Elerman et al.[19] have recently reported the magnetism of a dinuclear triply phenoxo bridged dinickel(II) complex which is of the face-sharing bioctahedral type. The Ni−O−Ni angles range from 86.2 to 88.3° which is close to 90°, and the Ni···Ni distance is at 2.884 Å. A *ferromagnetic* exchange coupling ($J = +11.5$ cm^{-1}) has been reported and interpreted in terms of a superexchange pathway.

Exchange coupling in the cobalt(II) complexes **6** and **7** with local high-spin d^7 configuration at the cobalt(II) ions is antiferromagnetic and within experimental error of identical magnitude in both species. It is conceivable that the expected diminished direct exchange going from **6** to **7** (due to the increasing Co···Co distance) is compensated by a more effective σ-superexchange pathway in the tris(μ-bromo) complex. A more detailed analysis is not possible at this point because the order of the a_1 and e orbitals in C_3 symmetry (Figure 7) is not known.

In the following we analyze the electronic structures of **5** and Sobota's complex which both contain the tris(μ-chloro)-diferrous moiety but different terminal ligands. As pointed out, in trigonal symmetry the t_{2g} metal orbital split into a_1 and 1e (Figure 7). Mössbauer spectroscopy of Sobota's complex clearly shows that in this species a nearly unperturbed a_1 ground state prevails giving rise to an $a_1^2 1e^2 2e^2$ electronic configuration at the Fe^{II} ions. It is then immediately obvious that direct exchange via a_1 orbitals does not provide a suitable pathway for exchange because these are filled. The half-filled 1e and 2e magnetic orbitals yield according to the Goodenough−Kanamori rules[20] an antiferromagnetic interaction. Remarkably, the observed antiferromagnetic coupling is rather weak ($J =$

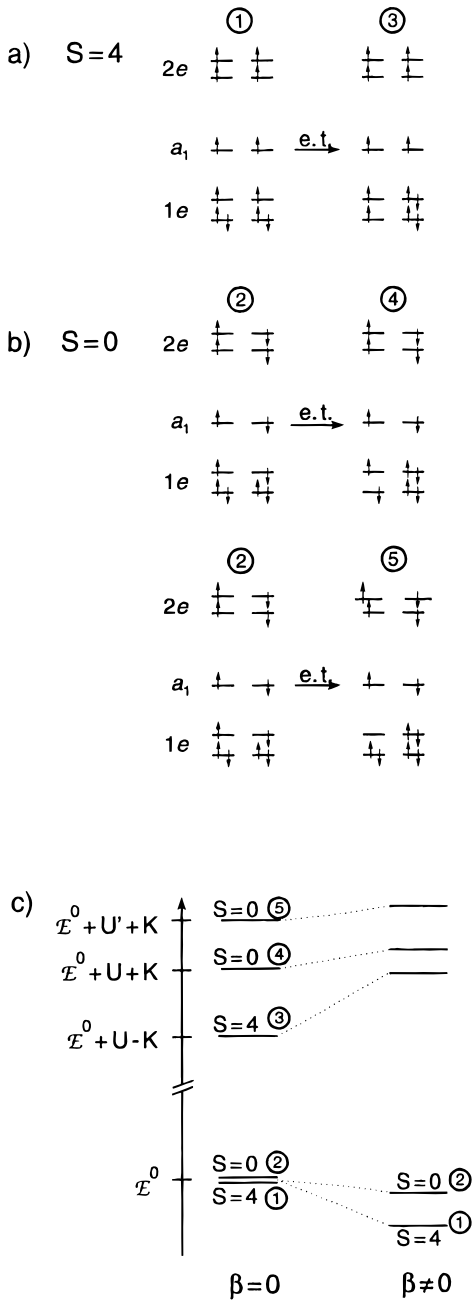

Figure 8. Generation of possible excited states 3−5 by one-electron transfer steps in the 1e orbitals assuming (a) parallel 1 or (b) antiparallel 2 spin alignment in the ground state of tris(μ-chloro)diferrous complexes. (c) Relative energies of the ground and excited states without interaction between the metal ions ($\beta = 0$) and with such interaction ($\beta \neq 0$).

(18) Hatfield, W. E. In *Theory and Applications of Molecular Paramagnetism*; Boudreaux, E. A., Mulay, L. N., Eds.; John Wiley & Sons: New York, 1976; p 352.
(19) Elerman, Y.; Kabak, M.; Svoboda, I.; Fuess, H.; Griesar,K.; Haase, W. *Z. Naturforsch.* **1996**, *51b*, 1132.
(20) (a) Anderson, P. W. *Phys. Rev.* **1950**, *79*, 350. (b) Goodenough, J. B. *Phys. Rev.* **1955**, *100*, 564. (c) Goodenough, J. B. *J. Phys. Chem. Solids* **1958**, *6*, 287. (d) Kanamori, J. *J. Phys. Chem. Solids* **1959**, *10*, 87. (e) Anderson, P. W. In Magnetism; Rado, G. T., Suhl, H., Eds.; Academic Press: New York, 1963; Vol. 1, Chapter 2. (f) Ginsberg, A. P. *Inorg. Chim. Acta* **1971**, *5*, 45.

-2 cm^{-1}) as compared to **3**, **4**, and **6**−**9**. A reason for this observation may be the differing terminal ligands (six tetrahydrofuran ligands in Sobota's complex vs two 1,4,7-trimethyl-1,4,7-triazacyclononane macrocycles in our complexes). This is corroborated by the data in Table 1. For $[(thf)_6Co_2(\mu\text{-}Cl)_3][SnCl_5(thf)]$ an antiferromagnetic coupling of $J = -1.7$ cm^{-1} has been reported whereas for **6** J is -13.1 cm^{-1}. Similarly, $J = -6$ cm^{-1} for $[(thf)_6Ni_2(\mu\text{-}Cl)_3][SnCl_5(thf)]$ and -10.5 cm^{-1} for **8**. Similar observations have been reported by Roman et al.[21] for a series of (μ-oxalato)dinickel(II) complexes with differing terminal ligands.

At this point it is not at all straightforward to find an additional *ferromagnetic* exchange pathway between two ferrous ions with a_1 ground state as is experimentally established for complex **5**.

From the Mössbauer spectra we had concluded that the local ground state of the Fe^{II} ions in **5** and Sobota's complex differ. The local ground state of an Fe^{II} ion in **5** is a mixture of a_1 (∼85%) and 1e (∼15%). We identify two possible origins for this orbital admixture in crystalline **5**: structural and electronic. (i) Due to packing effects in crystalline **5** the local symmetry at each iron(II) site is less than trigonal. This has been verified by the crystal structure determination of **5**. In Sobota's complex, on the other hand, the symmetry is much closer to C_{3v}. A pure a_1 ground state can only exist in C_3 symmetry, and lowering the symmetry facilitates mixing of wave functions a_1 and 1e. (ii) It should also be considered that the donor atoms of the terminal ligands in **5** are six pure σ-donors (tertiary nitrogen atoms) whereas there are six oxygen donor atoms in Sobota's complex (thf) which may exert some π-donor capability in addition to being good σ-donors. π-Donation destabilizes the 1e orbitals in Sobota's complex and increases the energy difference between the a_1 and 1e orbitals. Thereby, mixing of these orbitals becomes less effective as compared to the situation in **5**.

Now we focus on exchange pathways in a pure 1e configuration. Figure 8 gives the energetically lowest excited states, which can be generated by an intramolecular one-electron transfer,[20a] taking into account parallel or antiparallel spin coupling between the two ferrous ions. Configurations 1 and 2 are degenerate states neglecting the necessary resonance integral β_{ii} for coupling, but the excited states 3−5, which correspond to metal−metal charge transfer configurations, are energetically split due to intraatomic exchange, K, and double orbital occupation (Figure 8c). The energy of the excited state 5 is larger than that of 4 because one orbital of the Fe^{III} site in 5 is occupied by two electrons in contrast to 4 where each orbital is only half-filled. The Coulomb repulsion, U', of two electrons in one orbital exceeds that of two electrons in two orbitals U ($U' > U$). The interaction parameter β_{ii} mixes then the ground subspace with the excited one in a fashion that lifts the degeneracy of the ground space.[22] The magnitude of stabilization of 1, or 2 is then inversely proportional to the energy difference to the excited states. Excited state 3 with $S = 4$ is lowest in energy, and consequently, the $S = 4$ ground state of **5** is more stabilized than the corresponding $S = 0$ state.

In the foregoing discussion we have ignored the possible influence of the potential exchange which exhibits always a smaller ferromagnetic contribution than kinetic exchange.[20] We assume that in **5** and Sobota's complex the potential exchange contributions are very similar due to their similar core structures.

Acknowledgment. We thank the Fonds der Chemischen Industrie and the Deutsche Forschungsgemeinschaft (Schwerpunktprogramm "Bioanorganische Chemie") for financial support.

Supporting Information Available: Listings of crystallographic data, bond lengths and angles, anisotropic thermal parameters, and calculated positions of hydrogen atoms for complexes **1**, **3**, **5**, **6**, **8**, and **9** (66 pages). Ordering information is given on any current masthead page.

IC970119H

(21) Roman, P.; Guzman-Miralles, C.; Luque, A.; Beitia, J. I.; Cano, J.; Lloret, F.; Julve, M.; Alvarez, S. *Inorg. Chem.* **1996**, *35*, 3741.

(22) Hotzelmann, R.; Wieghardt, K.; Flörke, U.; Haupt, H.-J.; Weatherburn, D. C.; Bonvoisin, J.; Blondin, G.; Girerd, J.-J. *J. Am. Chem. Soc.* **1992**, *114*, 1681.

(23) Casey, A. T.; Mitra, S. In *Theory and Applications of Molecular Paramagnetism*; Boudreaux, E. A., Mulay, L. N., Eds.; John Wiley & Sons: New York, 1976; pp 109, 110.

(24) Gütlich, P.; Link, R.; Trautwein, A. X. In *Mössbauer Spectroscopy and Transition Metal Chemistry*; Springer-Verlag: Berlin, Heidelberg, New York, 1978.